Appl. Phys. B 80, 661–667 (2005)
DOI: 10.1007/s00340-005-1787-4

Applied Physics B
Lasers and Optics

T.A. PLANCHON✉
F. BURGY
J.-P. ROUSSEAU
J.-P. CHAMBARET

3D Modeling of amplification processes in CPA laser amplifiers

Laboratoire d'Optique Appliquée, Ecole Nationale Supérieure de Techniques Avancées,
Ecole Polytechnique CNRS UMR 7639 Chemin de la Hunière, 91761 Palaiseau Cedex, France

Received: 14 September 2004 /
Revised version: 16 February 2005 /
Published online: 30 March 2005 •

ABSTRACT We present here chirped pulse amplification simulations allowing for the extension of the generally used 1D model. The importance of the beam spatial profiles, diffraction and thermal effects in simulations is clearly shown in order to describe with accuracy the gain saturation. Experimental measurements performed on a 100 TW laser validate this calculation. The effects of dispersion and self-focusing are also studied.

PACS 42.60.By; 42.60.Da; 42.64.Re

1 Introduction

Ultra-short and ultra-intense laser pulses are currently produced from laser systems based on chirped pulse amplification (CPA) [1]. The generation of very short pulse width relies on broadband amplifying medium such as titanium-doped sapphire. Peak powers as high as 100 TW at 10 Hz [2] and 0.85 PW at a lower repetition rate [3] were obtained with this medium. Such systems have a front-end oscillator, a pulse stretcher, several stages of multipass or regenerative amplifiers, and a pulse compressor. The stretcher increases the duration of the pulse by a factor of 10^3–10^4 by introducing a frequency chirp in the pulse. After amplification the pulse is compressed to obtain temporal compression down to its original duration. In increasingly complex CPA systems, the need is to obtain the most energetic pulse without distorting the spatial and the temporal characteristics of the primary generated pulse.

The modeling of the complex amplifying process is of first importance to design such systems. Amplification theories rely on a semi-classical approach in which the active medium is generally described by the density matrix formalism and the field by the Maxwell equations. For solid-state amplifiers optical pulse duration is much longer than the polarization coherence time, so a quasi-static approximation can be made, thus giving a pair of rate equations. This approximation then leads to the so-called Frantz–Nodvik model [4, 5], which was first developed for monochromatic light. This model can be extended to broad spectrum chirped pulses by use of the instantaneous frequency formalism [6, 7], valid for highly stretched pulses. Generally, a uniform gain zone and a uniform amplified beam are assumed, leading to one dimensional simulations (1D-model) and multipass amplifiers analysis [4–8].

The aim of this paper is to investigate the validity of this 1D approach, to extend the amplification model to transverse (x and y) dimensions, and to study the influence of physical parameters (nonlinear index n_2, thermal load, diffraction) on the amplification calculation. The pump and seed beam characteristics of a 100 TW laser are measured to determine the initial gain, the initial injected (seed) beam in the amplifier chain, thermal lensing, and also to compare after each pass the evolution (energy, spatial and spectral profiles) of the real beam with the simulated one. The only remaining (not measured) parameter of the simulation is the saturation fluence of amplifying medium that was found from Ref. [9, 10]. We will show that taking into account the beam diffraction gives a very predictive model for spectral and spatial beam evolution during the amplification process, whereas the 1D-model gives only qualitative results and can only be used with arbitrary adjustment of the beam diameters or saturation fluence.

One-dimensional amplification model is first presented in Sect. 2. Based on a simple intensity evolution equation through a single pass in an amplifying medium, the 1D-model is extended to include chirped pulse amplification as well as multipass amplification. Some experimental data performed on a 100 TW laser are then presented, showing the limitations of 1D-model for treating amplification when saturation occurs. Section 3 presents a more complex model, based on nonlinear Schrödinger equation, which takes into account transverse sampling of gain and amplified beam, diffraction, thermal lensing in amplifiers, dispersion and nonlinear effects due to nonlinear index n_2. A nonlinear propagation and amplification software named CommodPro [11], issued from the MIRO code [12], is used to numerically solve this equation.

2 One-dimensional model

2.1 *Amplification for one pass through the medium*

The rigorous description of laser pulse amplification starts with solving the Maxwell equations for the electric

✉ Fax: 734-764-4876, E-mail: tplancho@mines.edu

field and considering the amplifying medium as a resonant two-level system. This leads to a propagation equation for the field and two equations for macroscopic polarization and population difference N [13]. In these equations, the times T_1 and T_2, respectively, the relaxation and the coherence time, are introduced. If all resonant atoms are initially in the upper level, the time T_1 corresponds to the lifetime of upper level, whose population then follows an exponential decreasing law. The coherence time T_2 describes the loss of phase coherence between the microscopic dipoles and is responsible for physical phenomena as the Rabi oscillations, auto-induced transparency or photon echo [13–15]. If the variations of the field envelope and of the population inversion are negligible during the time T_2 and if the variation due to spontaneous emission is neglected, then the equations for the field, population inversion and polarization can be written as a function of N and the laser intensity $I \equiv (\varepsilon_0 c/2)|E|^2$ as follows [16]:

$$\frac{\partial I}{\partial t} + c\frac{\partial I}{\partial z} = \sigma_e(\omega) c N I \tag{1}$$

$$\frac{\partial N}{\partial t} = -\frac{2^* \sigma_e(\omega)}{\hbar\omega} c N I \tag{2}$$

Here $\sigma_e(\omega)$ is the emission cross section of the laser transition which can be approximated, for homogeneous emission lines, by a Lorentzian shape $\sigma_e(\omega) = \frac{\sigma_a}{1+T_2^2(\omega-\omega_a)^2}$, with σ_a the value at resonance. The constant 2^* in (2) is used for generality of the equation. For a three-level laser medium, $2^* = 2$ and for a four-level laser medium, $2^* = 1$. In order to obtain the so-called Frantz–Nodvik equation from these two equations, some mathematical integrations are necessary [4, 5] thus yielding:

$$I(z,t) = I_0(t) \times \left[1 - \left(1 - G_0^{-1}\right)\exp\left(-\frac{J_0(t)}{J_{sat}}\right)\right]^{-1} \tag{3}$$

This equation gives the intensity profile $I(z, t)$ at distance z in an amplifier medium, as a function of the entrance intensity $I_0(t)$ and the parameters of the medium, σ_a and $N(z)$. $G_0 = \exp(\sigma_a \int_0^z N(z')dz')$ is called small signal gain. $J_{sat} = (\hbar\omega_a)/(2^*\sigma_a)$ is the saturation fluence of the medium. $J_0(t) \equiv \int_0^t I_0(t')dt'$ is the instantaneous fluence, corresponding to the number of photons by unit area in the pulse until time t, and it simply becomes the pulse fluence (in J m^{-2}) when t goes to infinity.

2.2 *Extension to multipass and CPA amplifiers*

To use (3) for multipass amplifiers, one needs to calculate the residual small signal gain after each pass and iterate. Supposing that the small signal gain $G_0^{(p)}$ and the intensity profile $I^{(p)}(t)$ are known for the (p)th pass, the intensity profile for the next pass $(p+1)$th is calculated with the Eq. (3) at $z = L$ (L being the crystal length). The residual gain after the (p)th pass can then be written as:

$$G_0^{(p+1)} = \exp\left[\frac{J_{sat}\ln\left(G_0^{(p)}\right) - \left(J_0^{(p+1)}(\infty) - J_0^{(p)}(\infty)\right)}{J_{sat}}\right] \tag{4}$$

The term $J_{sat}\ln(G_0^{(p)})$ corresponds to the energy density stored in the medium before the (p)th pass and the second term, $(J_0^{(p+1)}(\infty) - J_0^{(p)}(\infty))$, corresponds to the energy density extracted from the medium at this pass. For calculating the multipass amplification, the optical losses must also be taken into account.

The Frantz–Nodvik equation is sometimes used in a form linking the output fluence to the fluence before the medium:

$$J_L(t=\infty) = J_{sat} \times \ln\left[1 + G_0 \times \left(\exp\left(\frac{J_O(t=\infty)}{J_{sat}}\right) - 1\right)\right] \tag{5}$$

This equation is used in simple analysis for multipass amplifiers [8]. Equation (3) allows, on the other hand, the calculation of the temporal profile deformations caused by the laser transition saturation.

Now to extend the model to chirped pulses, the linear correspondence between time and frequency has to be used. This relation can be written as $\omega(t) = \omega_L + 2bt$, ω_L is the spectrum central frequency and b is the chirp factor (in s^{-2}). This linear relation is valid when the stretching factor is high, which is the case for Ti:sapphire lasers for which the initial pulse width is some tens of femtoseconds and after stretching it becomes hundreds of picosecond. It is also necessary to insert into Eq. (3) the spectral dependence of $G_0(\omega)$ and $J_{sat}(\omega)$ given by the frequency-varying emission cross section. For Ti:sapphire a Poisson distribution can be used [17] at 300 K for the stimulated emission cross section. We choose to use a Lorentzian fit from this Poisson distribution, which provides the values of the coherence time ($T_2 = 2.73$ fs) and resonant wavelength ($\lambda_a = 794$ nm). The value of stimulated emission cross-section σ_a at resonance is taken to be 3×10^{-19} cm^2 [9, 10].

With the Eq. (3) and the adaptation for broad spectrum, two phenomena known as gain narrowing and gain shifting can be described. The spectral narrowing of the amplified beam is caused by the frequency dependence of the gain, causing a better amplification at the resonant wavelength λ_a. The gain shifting effect is caused by saturation. The front of the pulse temporal profile is stronger amplified thus leading to spectrum changes due to the linear relation between time and frequency.

2.3 *Parameters for 1D simulation*

The previous 1D-model, assuming a uniform gain zone and a uniform amplified pulse with no transverse sampling, is the most commonly used model to simulate CPA amplification [4–8]. In this model, the laser beam needs to be defined after the stretcher by the three following parameters: its spectral profile, linear frequency chirp b, and fluence. The frequency chirp parameter b is determined by the following equation:

$$b = \frac{\Delta\omega}{2\Delta t_{et}} = \frac{\pi c \Delta\lambda}{\Delta t_{et}\lambda_L^2} \tag{6}$$

with $\Delta\lambda$, Δt and $\Delta\omega$, respectively, the full width half maximum values of the pulse in wavelength, time and frequency. λ_L

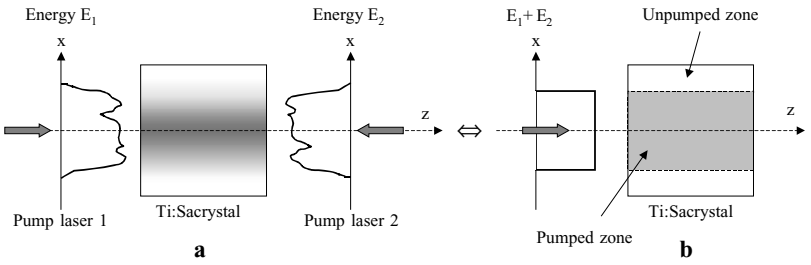

FIGURE 1 Pumping geometry. **a** real and **b** considered for 1D gain calculation

is the central wavelength of the pulse spectrum. The stretched pulse duration Δt_{et} can be determined for a large stretching factor by knowing the quadratic phase $\varphi^{(2)}$ given by the stretcher:

$$\Delta t_{et} = \left(\frac{4\ln 2}{\Delta t_0} \left| \varphi^{(2)}(\omega_L) \right| \right) \tag{7}$$

Lastly, to be able to define the beam fluence, an equivalent area S is used, giving the same energy and the same peak intensity. For a gaussian profile, this area is written:

$$S = \iint \exp(-2r^2/w^2) r \, dr \, d\theta = (\pi w^2/2) \tag{8}$$

For the 1D small signal gain calculation, the population inversion is taken uniform in x, y and z and is written N_0. The pump lasers (ns pulsed Nd:YAG @ 532 nm) are simulated by a beam whose energy is the sum of the individual beam energies (if more than one beam are used) as shown in Fig. 1. The pump fluence is then obtained by calculating the equivalent area of the pump beam.

The small signal gain is calculated as a function of the stored energy density J_{sto} in the active medium, using the equation:

$$G_0 = \exp\left(\frac{\hbar \omega N_0 L}{J_{sat}(\omega)} \right) = \exp\left(\frac{J_{sto}(\omega)}{J_{sat}(\omega)} \right) \tag{9}$$

The stored energy density is then given by :

$$J_{sto}(\omega) = A J_p \eta_c (\lambda_p / \lambda_L) \tag{10}$$

J_p is the fluence of the pump laser, A the absorption factor of this pump and η_c is called the quantum efficiency and describe the loss of gain due to non-radiative transitions in Ti:sapphire. This parameter represents the percentage of excited ions involved in the radiative transition. A curve fit from experimental data in Ref. [18] gives the following dependence of η_c on temperature,

$$\eta_c = \left[1 + \frac{T_{1rad}}{T_{1nr}} \exp\left(\frac{-\Delta E}{k_B T} \right) \right]^{-1}, \tag{11}$$

where $\Delta E = 1794\ \text{cm}^{-1}$, $T_{1rad} = 3.97\ \mu\text{s}$ and $T_{nr} = 2.93\ \text{ns}$.

Finally, as was mentioned in Sect. 2.1, a Lorentzian shape for emission cross section is used with the resonance value as $\sigma_e(\lambda_a) = 3.10^{-19}\ \text{cm}^2$ [9, 10], giving saturation fluence at resonance $J_{sat} = 0.844\ \text{J cm}^{-2}$. The small signal values determined with Eqs. (9) and (10) are shown in Table 1.

	1st amplifier	2nd amplifier	3rd amplifier
Pump surface S (cm^2)	1.6×10^{-3}	8.7×10^{-2}	1.1
Pump fluence J_p (J cm^{-2})	4	2.3–2.7	3.2
$G_0(\omega_a)$	10	4–5	8.4
η_c	0.8	0.8	1

TABLE 1 Parameters used for 1D simulations. $\eta c = 1$ for cooling down to 120 K. Parameters correspondence to 100 TW LOA laser

2.4 *Comparison with experimental measurements*

In order to check the validity of the results given by the model, extensive measurements performed on a 100 TW/10 Hz laser are used to determine the parameters presented in Sect. 2.3 and to compare after each pass the evolution of the real beam with the simulated one. This 100 TW laser [2] is made of three consecutive multipass amplifiers leading after compression to 2.5 J in 25 fs.

By looking at the simulated spectral profiles obtained with the 1D-model, it appears that they only match the experimental profiles for the first amplifier where nearly no saturation occurs. The calculated energies and the comparison with experimental values are presented in Fig. 2. This figure clearly shows that when saturation occurs, for second and third amplifiers, the 1D-model is not able to describe the energy growth. For the first few passes in these two amplifiers, there is a good correspondence between simulated and experimental energies, meaning that the small signal gain values of Table 1 are correct.

These small signal gain values are determined by the pump fluence J_p and the saturation fluence J_{sat}. Less saturation would be obtained for the same initial gain G_0 with a higher value of J_{sat} and a smaller value of J_p. The value of J_{sat} is taken from [9, 10] and the uncertainties on J_p, dues to the non-uniform pump spatial profiles, are not sufficient to explain the difference in energy in Fig. 2. In the next section, the introduction of the transverse spatial profile will remove the uncertainty on the pump fluence and confirm the value of the saturation fluence.

3 Three-dimensional model

3.1 *Model presentation*

On account of the limitations of the 1D-model presented before, it is required, for more precise description of the amplifying process, to take into account the spatial aspect of the amplified laser beam. The energy deposited by the

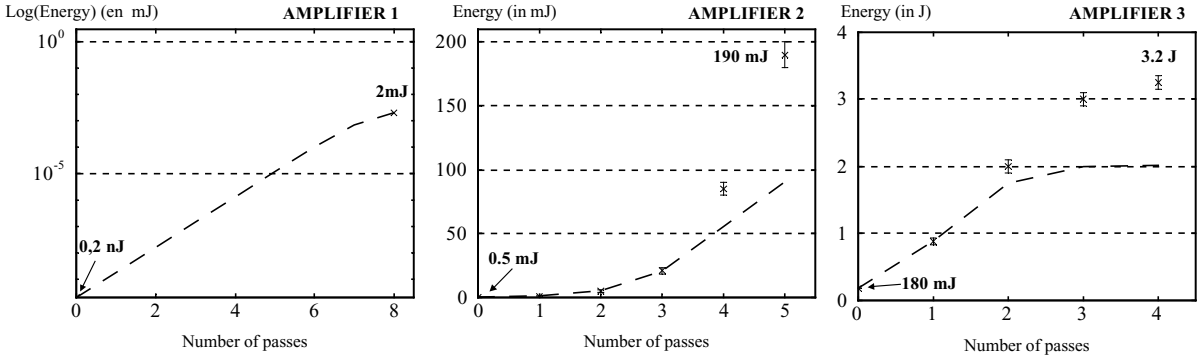

FIGURE 2 Energy evolution for the three amplifiers. Crosses are experimental measurements and doted lines the 1D simulation results

pump lasers in the amplifying medium needs to be calculated and then the above amplifying Frantz–Nodvik model with extension in the transverse spatial domain must be used. However, we also wanted to include in the model diffraction and nonlinear effects (optical Kerr effect) and study their influence on the amplification. It is then needed to resolve the coupled equations of amplification and nonlinear propagation simultaneously.

For the resolution of nonlinear propagation, the Maxwell equations for electromagnetic field lead to a propagation equation in nonlinear medium that is called nonlinear Schrödinger equation [14]:

$$\left[\underbrace{\frac{\partial}{\partial z}+k'\frac{\partial}{\partial t}}_{1}+\underbrace{\nabla_{\perp}^{2}}_{2}\underbrace{-i\frac{k''}{2}\frac{\partial^{2}}{\partial t^{2}}}_{3}+\underbrace{i\frac{k_2\left|E^{2}\right|}{2}}_{4}\right]\times E(x,y,z,t)=0 \tag{12}$$

The first term in (12) is the longitudinal propagation term, which describes the propagation toward z at the group velocity $v_g(v_g^{-1}=k')$. The second term describes the diffraction of the beam. The third term describes the effects given by the group velocity dispersion of the medium. The final term, with $k_2=(n_2w)/c$, takes into account the nonlinear index n_2 and then describes the phenomena that come from optical Kerr effect.

The thermal effects in amplifying medium are also considered. The heating of the crystal induced by its pumping creates a thermal lensing that is modeled by considering a perfect lens (quadratic phase mask) on the crystal. To evaluate the focal length, the following equation, which is found for a cylindrical crystal with r_1 being the radius of the pumped zone [19], is used:

$$f_{\mathrm{th}}=\frac{2\pi\cdot r_{\mathrm{i}}^{2}K}{P_{\mathrm{th}}\left[\left(\frac{dn}{dT}\right)_{T=T_0}+\frac{2r_2\,\alpha_{\mathrm{th}}(n_0-1)}{L}\right]} \tag{13}$$

L is the crystal length and n_0 its index at the temperature of the center of the crystal. $P_{\mathrm{th}}=A\,E_{\mathrm{p}}f_{\mathrm{rep}}(1-\eta_{\mathrm{c}}\frac{\lambda_{\mathrm{p}}}{\lambda_{\mathrm{L}}})$ is the thermal power, with E_{p} the pump lasers energy and f_{rep} their repetition rate. Some thermal parameters of Ti:sapphire are presented in Table 2.

To numerically solve Eq. (12) considering the amplification and thermal effects during the propagation, we use a nonlinear propagation and amplification software [11, 12]. The amplification is treated with the same equations as in Sect. 2.

Thermal conductivity K (W m^{-1} K^{-1})	46 (300 K), 150 (150 K)
(dn/dT) (K^{-1}) (extraordinary ary axis)	$\frac{dn}{dT}(T)=4.11\times10^{-6}-1.565\times10^{-10}\,T+6.449\times10^{-11}\,T^2$
Thermal expansion coefficient αth (K^{-1})	(5 to 6.6)10^{-6}

TABLE 2 Thermal parameters of Ti:sapphire

The small signal gain is calculated in three dimensions using the experimental pump spatial profiles. Different terms of Eq. (12) can be considered. In Sect. 3.2, the simulations are made with terms 1 and 2, so considering diffraction and thermal lensing. In Sect. 3.3, the thermal lensing is removed. The last section considers all the terms of the equation, including dispersion and nonlinear effect.

3.2 *Simulation with diffraction and thermal lensing*

In the 100 TW laser used for the measurements, thermal lensing in the first multipass amplifier has no effect since this amplifier is used in confocal geometry [20]. The third amplifier, pumped by 8 J of Nd:YAG laser, is cryogenically cooled and has no thermal lensing. For the second amplifier, the Eq. (13) gives for the thermal focal lens $f_{\mathrm{th}}=49$ m. Wavefront measurements realized with a Shack–Hartmann wavefront sensor at the entrance of the amplifier and after the 4th pass, gives a focal lens measured after the 4th pass equals to 14 m. By considering four passes in the thermal lensing with one meter propagation between each pass, a thermal lensing of 55 m is deduced. This last value is used in the simulation.

For 1D-model, only measured energy and spectral profile changes were compared with simulation. Now the spatial profiles of the injected laser beams are also used in the simulation. Figure 3 shows the spatial profiles in the last four-pass amplifier, where the changes in beam spatial profile are the most obvious. The simulated profiles are in very good agreement with measured ones. The transformation of the profile from a gaussian at the entrance of the amplifier to a supergaussian after the amplifier is clearly seen.

The calculated energies and the comparison with experimental values are presented in Fig. 4. This figure shows that the 3D-model is able to predict the energy evolution within error bars and that it perfectly describes the saturation in contrast with the 1D-model.

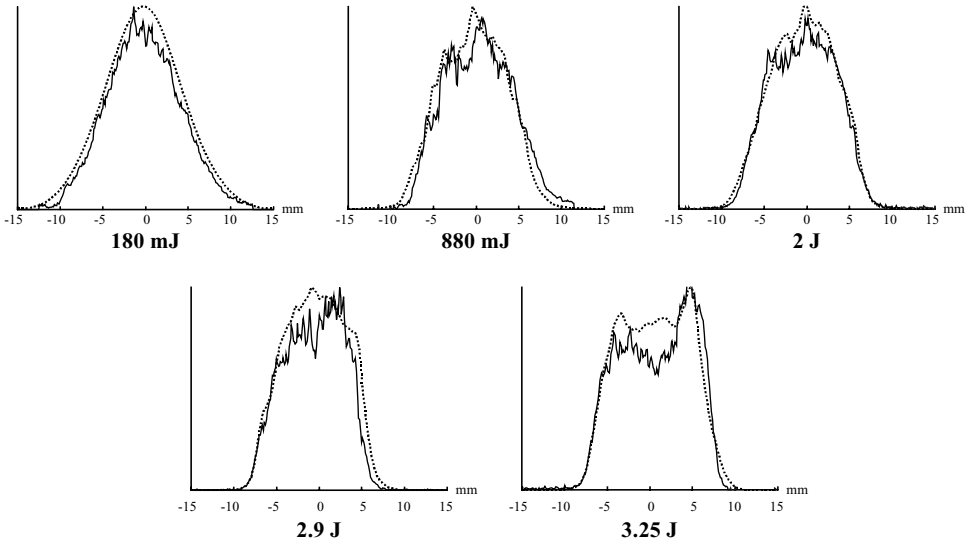

FIGURE 3 Spatial profile evolution in the last amplifier. *Solid line*: Experimental measurement. *Dashed line*: Simulated profile

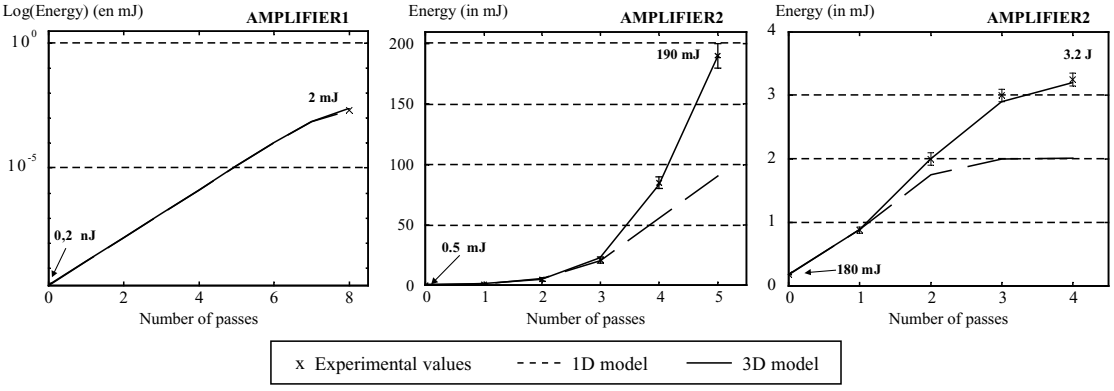

FIGURE 4 Energy evolution for the three amplifiers. Crosses are experimental measurements, *doted lines* the 1D simulation results and *solid lines* the 3D simulation results

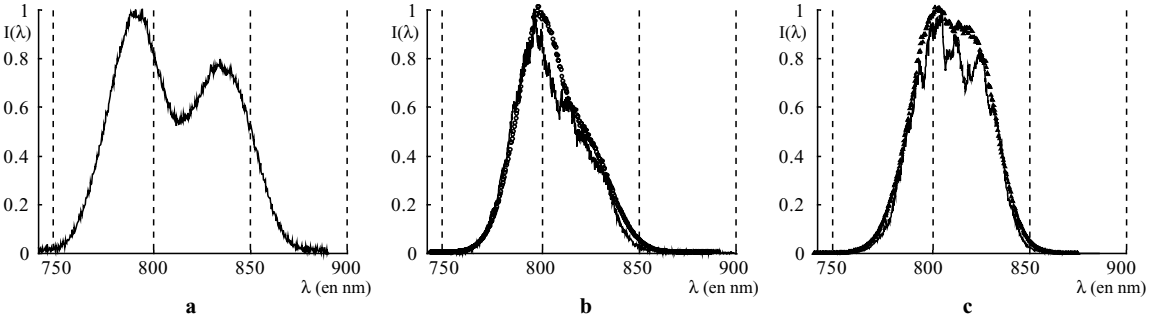

FIGURE 5 Comparison of experimental (*solid lines*) and simulated spectral profile of the infrared beam. **a** Oscillator spectrum modulated by Dazzler. **b** Spectrum after 2nd amplifier. **c** Spectrum after the 3rd amplifier

In order to be complete, the simulation also has to describe the transformation occurring on the spectral profile of the amplified beam. Figure 5 shows the spectral profile evolution in the laser chain when the initial spectrum is modulated with an acousto-optic device (Dazzler). Gain narrowing in the first amplifier is occurring, leading to spectrum narrowing (Fig. 5b). When saturation is important in the third amplifier, the spectrum is shifted toward longer wavelength (Fig. 5c). The simulated spectrum perfectly describes these two phenomena.

3.3 *Influence of thermal lensing*

To check the importance of thermal lensing in the calculation result, the amplification is calculated without the perfect lens that simulated the thermal lensing effect occurring in the second amplifier. Figure 6 shows measured and simulated spatial profiles for the last three passes of the second amplifier. Spatial profiles of Fig. 6b, with thermal lensing into account, are in good agreement with measured profiles (Fig. 6a), in term of shape and energy values. Otherwise, when

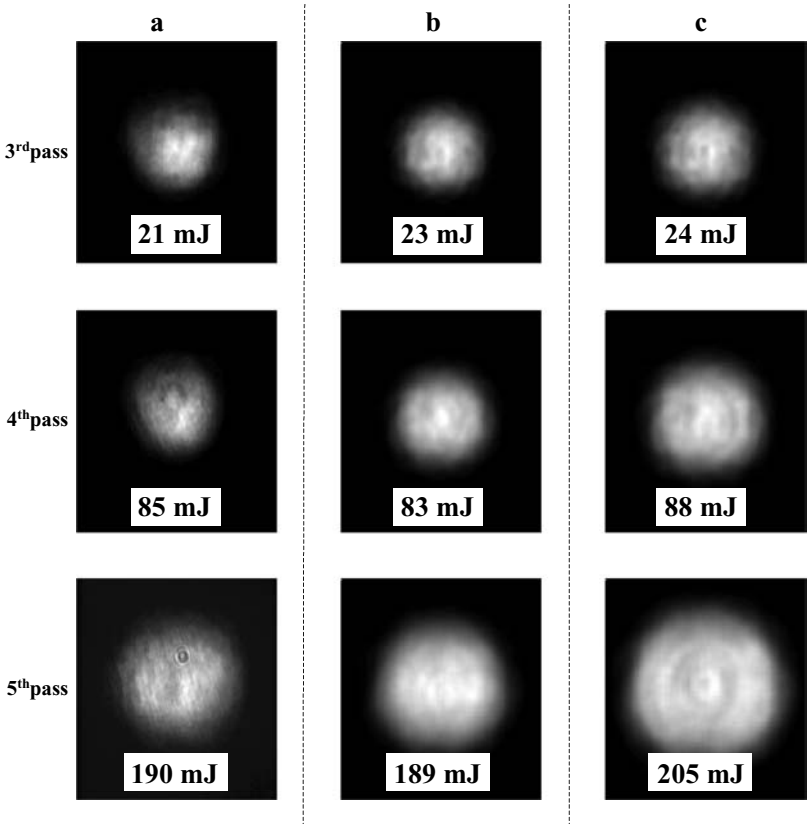

FIGURE 6 Spatial profiles in the 2nd amplifier for last three passes. **a** Experimental measurements **b** simulated spatial profiles with thermal lensing **c** simulated spatial profile without considering thermal lensing

the thermal lensing is not included (Fig. 6c), it clearly appears that the simulated profiles in that case do not agree with the experimental one. The energy values are also not corresponding to the real ones. The thermal lensing, when present, has a non-negligible effect on the amplification and it is important to include it in the model.

3.4 *Influence of dispersion and nonlinear index*

In this section, all the terms of Eq. (12) are considered, including dispersion and nonlinear effect. The dispersion is found to have no influence on the result, the temporal duration being quite long (600 ps after the stretcher). On the other hand, the nonlinear index ($n_2 = 5.210^{-20}\cdot$ m^2 W^{-1}, value for doped sapphire [21]) should induce a weak global self-focusing of the beam. Two simulations, with and without nonlinear effect, are made to check the importance of this self-focusing. The FWHM values (Φ_x and Φ_y) of the spatial profile after the second amplifier are compared for the two cases. A self-focusing is observed, the FWHM changing from $\Phi_x = 4.2$ mm and $\Phi_y = 5.1$ mm without nonlinear effect to $\Phi_x = 4$ mm and $\Phi_y = 4.9$ mm when taking into account n_2. This confirms that the nonlinear effect is negligible in comparison to the effect of the thermal lensing and could be ignored for calculation of amplification.

4 Conclusions

In this article, we have reviewed the different approaches for modeling the amplification in CPA laser chains. It was shown that the commonly used 1D-model is not predictive when saturation occurs. When taking into account the beam transverse profile, diffraction and thermal lensing, the model (called 3D-model) predicts the right values of the laser beam during the amplification. The effects of dispersion and self-focusing are of less importance and can be ignored in the calculation. On the other hand, the diffraction and thermal lensing have to be inserted in the model to obtain an accurate result. The only parameter that was not measured for our validation was the stimulated emission cross section. This study is also the first validation of the software used [11, 12] on a real size laser system.

Regarding these simulations results, we have also studied the possibility to adapt parameters in a 1D-model to see if it can be used instead of a 3D-model, which requires much more effort. The main difference between 1D and 3D simulations is the better description of saturation. It is then possible to obtain right values of amplified beam energies with 1D-model, when adapting the equivalent surface of the beam that was calculated using Eq. (8). It will then decrease beam fluence and saturation. Even if this adaptation of the beam equivalent surface is not very rigorous, when we search for a factor to multiply surface in Eq. (8) for our laser system, we find a different factor to use for each amplifier, 2.3 for second amplifier and 1.4 for third amplifier. It can be concluded that 1D-model is not a predictive model, the factor to adapt for saturation description varying according to the amplifier geometry and number of passes. Nevertheless, the 1D-model can have some utilities for an existing laser chain, for example, to calculate quickly spectrum modification (gain narrowing and shifting) when modulating the spectral amplitude of the injected beam

at the beginning of laser, right after stretcher. This model can be used in that particular case.

ACKNOWLEDGEMENTS The authors would like to thank Dr. W. Amir for helpfull discussions about the models.

REFERENCES

1 D. Strickland, G. Mourou, Opt. Commun. **56**, 219 (1985)
2 M. Pittman, S. Ferré, J.-P. Rousseau, L. Notebaert, J.P. Chambaret, G. Chériaux, Appl. Phys. B **74**, 529 (2002)
3 M. Aoyama, K. Yamakawa, Y. Akahane, J. Ma, N. Inoue, H. Ueda, H. Kiriyiama, Opt. Lett. **28**(17), 1594 (2003)
4 L.M. Frantz, J.S. Nodvik, J. Appl. Phys. **34**, 2346 (1963)
5 R. Bellman, G. Birnbaum, W.G. Wagner, J. Appl. Phys. **34**, 780 (1963)
6 C. Le Blanc, P. Curley, F. Salin, Opt. Commun. **131**, 391 (1996)
7 Y.H. Cha, Y.I. Kang, C.H. Nam, J. Opt. Soc. Am. B **16**, 1220 (1999)
8 W.H. Lowdermilk, J.E. Murray, J. Appl. Phys. **51**, 2436 (1980)
9 P.F. Moulton, J. Opt. Soc. Am. B **3**, 125 (1986)
10 G.F. Albrecht, J.M. Eggleston, J.J. Ewing, Opt. Commun. **52**, 401 (1985)
11 Technical details can be found on : www.oxalis-laser.com
12 O. Morice, Opt. Eng. **42**, 1530–1541 (2003)
13 G.L.J. Lamb, Rev. Mod. Phys. **43**(2), 99 (1971). For propagation equation, see Eq. (2.1). For macroscopic polarization and population difference, see appendix A
14 A.E. Siegman "LASERS". For nonlinear Schrödinger equation, see Chap. 10 (1986)
15 A. Icsevgi, W.E. Lamb, Phys. Rev. **185**(2), 517 (1969)
16 N.G. Basov, R.V. Ambartsumyan, V.S. Zuev, P.G. Kryukov, V.S. Letokhov, Sov. Phys.—JETP **23**(1), 16 (1966)
17 J.M. Eggleston, L.G. DeShazer, K.W. Kangas, IEEE J. Quantum Electron. **24**, 1009 (1988)
18 C.E. Byvik, A.M. Buoncristiani, IEEE J. Quantum Electron. **21**, 1619–1624 (1985)
19 W. Koechner, Heat removal, *Solid-State Laser Engineering* (Springer, Berlin, 1999), Chap. 7
20 P. Georges, F. Estable, F. Salin, J.P. Poizat, P. Grangier, A. Brun, Opt. Lett. **16**, 144–146 (1991)
21 S. Smolorz, F. Wise, Opt. Lett. **23**, 1381–1383 (1998)